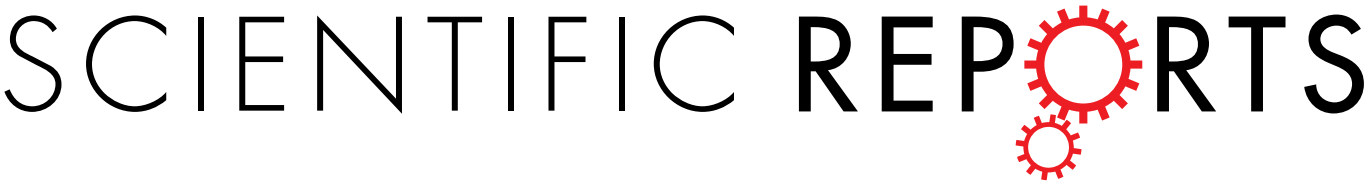

OPEN

Origin of Symmetric Dimer Images of Si(001) Observed by Low-Temperature Scanning Tunneling Microscopy

Received: 17 March 2016
Accepted: 26 May 2016
Published: 13 June 2016

Xiao-Yan Ren[1,2,3], Hyun-Jung Kim[2,4], Chun-Yao Niu[1,5], Yu Jia[1,5] & Jun-Hyung Cho[1,2,6]

It has been a long-standing puzzle why buckled dimers of the Si(001) surface appeared symmetric below ~20 K in scanning tunneling microscopy (STM) experiments. Although such symmetric dimer images were concluded to be due to an artifact induced by STM measurements, its underlying mechanism is still veiled. Here, we demonstrate, based on a first-principles density-functional theory calculation, that the symmetric dimer images are originated from the flip-flop motion of buckled dimers, driven by quantum tunneling (QT). It is revealed that at low temperature the tunneling-induced surface charging with holes reduces the energy barrier for the flipping of buckled dimers, thereby giving rise to a sizable QT-driven frequency of the flip-flop motion. However, such a QT phenomenon becomes marginal in the tunneling-induced surface charging with electrons. Our findings provide an explanation for low-temperature STM data that exhibits apparent symmetric (buckled) dimer structure in the filled-state (empty-state) images.

Over the last 30 years the atomic and electronic structures of the Si(001) surface have been extensively investigated because of the fundamental building block for the fabrication of electronic devices as well as for the prototypical model system of semiconductor surfaces[1–8]. From enormous experimental and theoretical studies, it is well established that the basic reconstruction of Si(001) consists of the formation of buckled dimers[9–12]. However, at room temperature scanning tunneling microscopy (STM) experiments showed symmetric dimer images because of a thermally activated flip-flop motion of buckled dimers. Such apparent symmetric dimer images disappear below ~120 K[13], forming either the $c(4 \times 2)$ structure [see Fig. 1(a)] consisting of alternatively buckled dimers along and perpendicular to the dimer rows or the $p(2 \times 2)$ one with alternatively buckled dimers along the dimer rows. Surprisingly, further cooling below ~20 K causes the buckled dimers to appear symmetric again[14,15]. Such symmetric-dimer STM images at low temperature have been explained in terms of various origins such as a dynamical flip-flop motion of buckled dimers[15,16], local surface charging effects[17], a possible asymmetric $p(2 \times 1)$ reconstruction[18], an inelastic tunneling mechanism via electron-vibration coupling[19], and a contribution of bulk states[20,21]. However, the microscopic mechanism underlying the low-temperature symmetric dimer images has remained an open question.

There have so far been a number of low-temperature STM experiments to characterize the apparent symmetric dimer images. Yokoyama and Takayanagi[15] observed the symmetric dimer images at 5 K with both positive and negative bias voltages, which were explained by slow dynamical flip-flop motion of the buckled dimers during the STM scan. Mitsui and Takayanagi[16] found that at 65 K higher tunneling currents increase not only the area of symmetric dimer images but also the flip-flop rate of buckled dimers regardless of the polarity of the bias voltage.

[1]International Laboratory for Quantum Functional Materials of Henan, and School of Physics and Engineering, Zhengzhou University, Zhengzhou 450001, China. [2]Department of Physics and Research Institute for Natural Sciences, Hanyang University, 17 Haengdang-Dong, Seongdong-Ku, Seoul 133-791, Korea. [3]School of Mechanical and Electrical Engineering, Henan Institute of Science and Technology, Xinxiang 453003, China. [4]Korea Institute for Advanced Study, 85 Hoegiro, Dongdaemun-gu, Seoul 130-722, Korea. [5]Center for Advanced Analysis and Computational Science, Zhengzhou University, Zhengzhou 45001, China. [6]International Center for Quantum Design of Functional Materials (ICQD), HFNL, University of Science and Technology of China, Hefei, Anhui 230026, China. Correspondence and requests for materials should be addressed to Y.J. (email: jiayu@zzu.edu.cn) or J.-H.C. (email: chojh@hanyang.ac.kr)

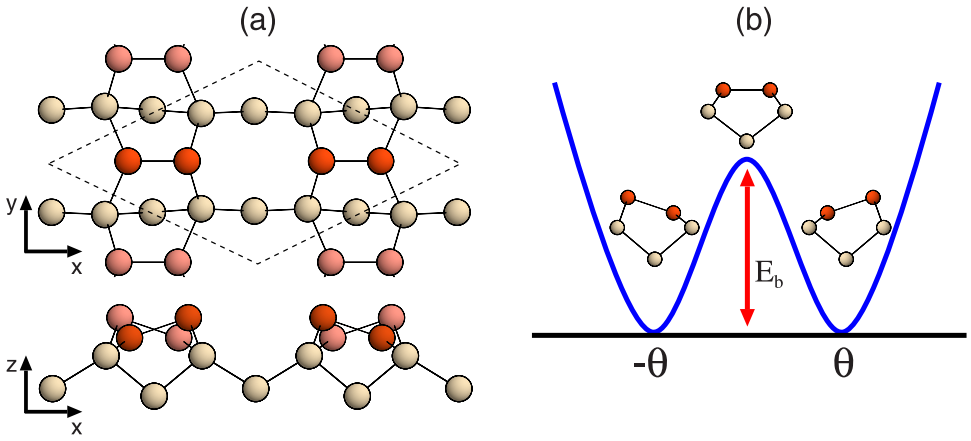

Figure 1. (**a**) Top and side views of the optimized $c(4 \times 2)$ structure of Si(001). The $c(4 \times 2)$ unit cell is indicated by the dashed line. The **x** (**y**) axis is perpendicular (parallel) to dimer rows, while the **z** axis is along the [001] direction. For distinction, the Si-dimer atoms within and outside the $c(4 \times 2)$ unit cell are drawn with two different dark circles. In (**b**), the symmetric double-well potential for the flipping of buckled dimers is schematically drawn. Here, E_b denotes the energy barrier, obtained by the energy difference between the $p(2 \times 1)$ and $c(4 \times 2)$ structures.

However, Ono *et al.*[17] observed both buckled and symmetric dimer images depending on the polarity of the bias voltage below 10 K: i.e., the buckled dimer images, locally forming $c(4 \times 2)$ or $p(2 \times 2)$ periodicity, were observed with positive bias voltages (empty-state images), while most of the dimers appear symmetric with negative bias voltages (filled-state images). Subsequent low-temperature STM experiments[22–24] confirmed buckled dimer structure in the empty-state images and apparent symmetric dimer structure in the filled-state images. Interestingly, a recent STM study of Manzano *et al.*[21] reported that at 7 K the negative bias voltages smaller than −1.5 V remained a $c(4 \times 2)$ reconstruction, but those larger than −1.5 V produced symmetric dimer images. On the basis of existing low-temperature STM data[15–17,21], the following questions on the appearance of symmetric dimer images can be raised: i.e., Why does the activation barrier (E_b) for the flipping of buckled dimers become much reduced at low temperature? What is the reason why the filled-state and empty-state STM images exhibit symmetric and buckled dimer structures, respectively? How does the tunneling-induced surface charging at low temperature[17,25,26] or the electric field via bias voltage affect STM imaging to show apparent symmetric dimer structure?

In this paper, we perform first-principles density-functional theory (DFT) calculations to investigate the energy difference [equivalently E_b as shown in Fig. 1(b)] between the symmetric-dimer structure and the $c(4 \times 2)$ structure under electron or hole doping as well as in the presence of external electric field applied along the [001] direction. We find that, as the amount of hole doping increases, E_b decreases more dominantly than the case of electron doping. Compared to such surface charging effects, the application of electric field is found to give a relatively small change in E_b. As E_b decreases with hole doping, the thermally activated flipping rate of buckled dimers is still negligible below 10 K, but the quantum tunneling (QT) driven flip-flop motion can be enabled to produce the symmetric-dimer STM images. Such a QT phenomenon of buckled dimers is, however, marginal with electron doping. Thus, a long-standing puzzle about the appearance of symmetric dimer images in low-temperature STM experiments can be solved in terms of the QT-driven flip-flop motion of buckled dimers, which can be facilitated by the tunneling-induced surface charging with holes.

Results and Discussion

We begin to optimize both the symmetric dimer structure, forming a $p(2 \times 1)$ periodicity (hereafter, designated as the $p(2 \times 1)$ structure), and the $c(4 \times 2)$ structure. The optimized $c(4 \times 2)$ structure is displayed in Fig. 1(a). We find that the $c(4 \times 2)$ structure has a dimer bond length of $d_D = 2.357$ Å and a dimer buckling angle of $\theta = 18.0°$. This $c(4 \times 2)$ structure is found to be more stable than the symmetric-dimer structure by 255 meV per dimer, yielding $E_b = 255$ meV [see Fig. 1(b)]. As shown in Fig. 2(a,b), the calculated band structure of $p(2 \times 1)$ has a metallic band crossing the Fermi level E_F, whereas that of $c(4 \times 2)$ exhibits a semiconducting feature with a band gap E_g of 0.27 eV. The present results for the geometry, energetics, and band structure of the $c(4 \times 2)$ structure are in good agreement with those of previous DFT calculations[10,27].

It has been known in several metal-adsorbate systems on Si or Ge surfaces[25,26,28] that below ~40 K electrons or holes, injected through tunneling current in STM, result in surface charging due to a substantially suppressed charge transport between the surface layer and the semiconducting bulk. In order to examine the influence of surface charging on the energetics of the $p(2 \times 1)$ and $c(4 \times 2)$ structures, we perform total-energy calculations for the two structures with electron (whose amount is represented as a positive value of n_e) or hole doping. Figure 3 shows the calculated values of E_b as a function of n_e ranging from $-0.6e$ to $0.6e$ per $p(2 \times 1)$ unit cell. We find that both the electron and hole dopings reduce the energy difference between the $p(2 \times 1)$ and $c(4 \times 2)$ structures. The resulting decrease of E_b with electron or hole doping can be attributed to the metallic and semiconducting features of the $p(2 \times 1)$ and $c(4 \times 2)$ structures, respectively. As shown in Fig. 2(a,b), for the electron doping of

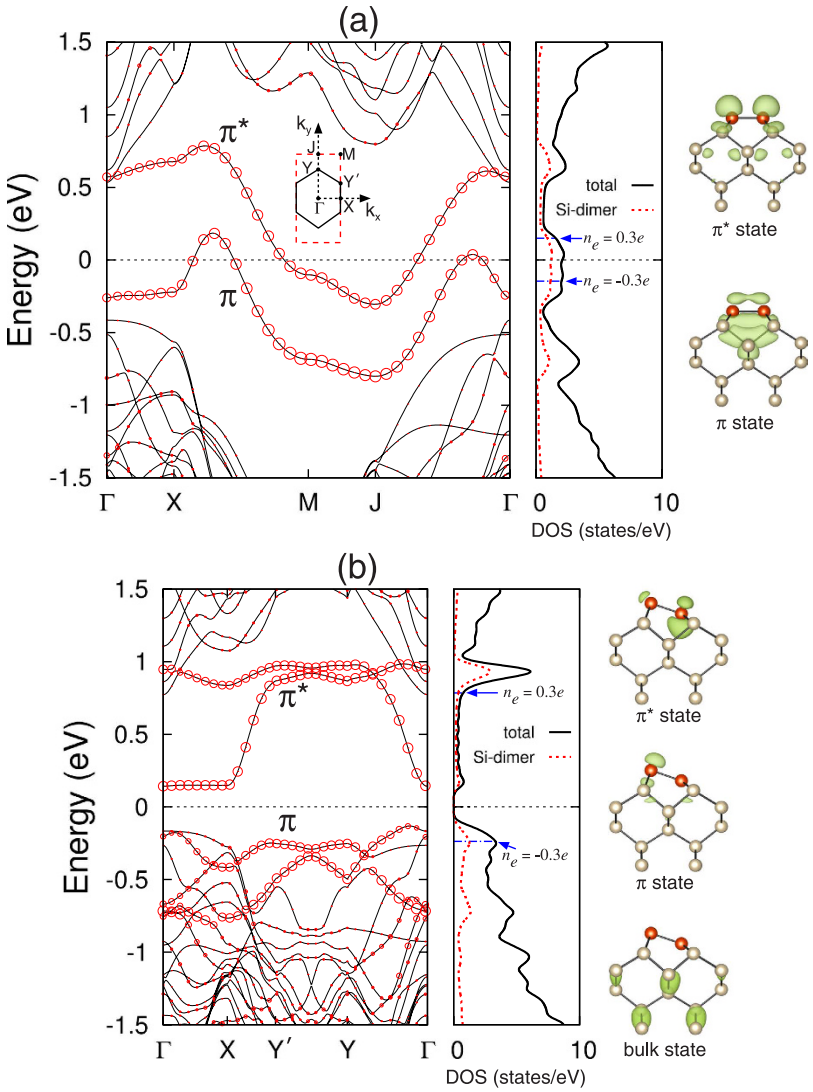

Figure 2. Calculated surface band structures of (**a**) the $p(2 \times 1)$ and (**b**) $c(4 \times 2)$ structures. The bands projected onto the p_x, p_y, and p_z orbitals of Si-dimer atoms are displayed with circles whose radii are proportional to the weights of such orbitals. The energy zero represents E_F. The inset in (**a**) shows the surface Brillouin zones of the $p(2 \times 1)$ and $c(4 \times 2)$ unit cells. The total DOS and the local DOS of Si dimers are displayed with solid and dotted lines, respectively. The charge characters of the π and π^* surface states at the Γ point are drawn with an isosurface of 0.05 e/Å, while that of the bulk state of $c(4 \times 2)$ at the Γ point (just below E_F) is drawn with an isosurface of 0.02 e/Å.

$n_e = 0.3e$, excess electrons in $p(2 \times 1)$ occupy the electronic states just above the Fermi level, while those in the semiconducting $c(4 \times 2)$ structure occupy the conduction band separated by a band gap of 0.27 eV from the valence band. Therefore, the total energy of the $p(2 \times 1)$ structure is expected to decrease more largely compared to the $c(4 \times 2)$ structure. On the other hand, for the hole doping of $n_e = -0.3e$, holes in $p(2 \times 1)$ are created in the electronic states just below the Fermi level, while those in $c(4 \times 2)$ are created in the relatively lower valence bands. One thus expects a larger increase in the total energy of the $c(4 \times 2)$ structure compared to the $p(2 \times 1)$ structure. The resulting decrease of the energy difference between the $p(2 \times 1)$ and $c(4 \times 2)$ structures under either electron or hole dopings leads to a decrease of E_b.

As shown in Fig. 3, E_b decreases more significantly with increasing hole doping, compared to the case of electron doping. This difference between electron and hole dopings may be explained in terms of the different characters of the unoccupied and occupied electronic states in the $p(2 \times 1)$ and $c(4 \times 2)$ structures: i.e., (*i*) the lowest unoccupied states in $p(2 \times 1)$ and $c(4 \times 2)$ are mostly the surface states of π^* orbitals and (ii) the highest occupied states in $p(2 \times 1)$ are the surface states of π orbitals, while those in $c(4 \times 2)$ consist of the surface states of orbitals as well as the bulk states [see the total density of states (DOS) and the local DOS of Si dimers in Fig. 2(a,b)]. It is found that, for hole doping with $n_e = -0.3e$, the majority of the holes in the $c(4 \times 2)$ structure is created in the bulk states around the Γ point [see Fig. 1S of the Supplemental Material], possibly giving rise to a relatively larger strain energy compared to the $p(2 \times 1)$ structure where holes are created mostly in the surface states. Here, we

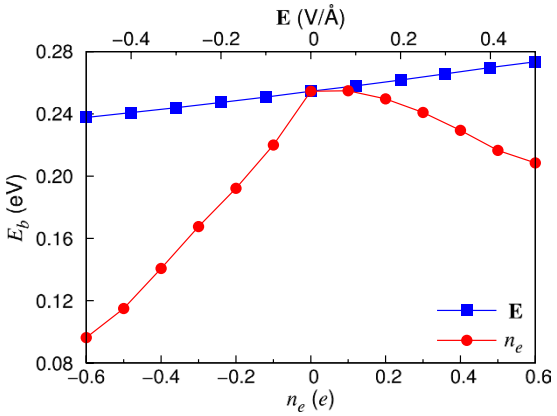

Figure 3. Calculated energy barrier E_b [see Fig. 1(b)] for the flip-flop motion of buckled dimers as a function of electron and hole dopings as well as external electric field. The unit of e in n_e is given per $p(2 \times 1)$ unit cell.

note that, since the atom in the interior of the bulk has more neighboring atoms and experiences relatively larger interaction forces from its surroundings than the surface atom[29], the hole-induced strain in $c(4 \times 2)$ is likely to yield a larger energy cost compared to the case of $p(2 \times 1)$. In this sense, we believe that hole doping decreases a more significant decrease of E_b, compared to electron doping where excess electrons in both the $c(4 \times 2)$ and $p(2 \times 1)$ structures are occupied mostly in their surface states.

Next, we examine the influence of external electric field **E** on the energetics of the $p(2 \times 1)$ and $c(4 \times 2)$ structures. Here, **E** is simulated by superimposing an additional sawtooth potential along the [001] direction (taken as the $+z$ direction) with discontinuity at the mid-plane of the vacuum region of the supercell. Note that an STM bias voltage of 1.5 V and a tip-sample distance of ~5 Å would give rise to an electrical field of ~0.3 V/Å. Figure 3 also shows the calculated values of E_b as a function of **E** ranging between −0.5 and +0.5 V/Å. We find that E_b increases (decreases) as **E** increases along the $+z$ ($-z$) direction. These different behaviors of E_b depending on the direction of **E** can be explained in terms of the different contributions of electrostatic energy due to external electric field between the $p(2 \times 1)$ and $c(4 \times 2)$ structures. Since the surface dipole moment p_z (pointing $-z$ direction) of the metallic $p(2 \times 1)$ structure is larger in magnitude by $\Delta p_z = 0.038\, e$Å than that of the semiconducting $c(4 \times 2)$ structure, an electric field applied along the $+z$ ($-z$) direction gives a positively (negatively) larger electrostatic energy $U = -\mathbf{p} \cdot \mathbf{E}$ of surface dipole in $p(2 \times 1)$ compared to in $c(4 \times 2)$, leading to an increase (decrease) of E_b. Here, we evaluate the difference of surface dipole moment Δp_z between the $p(2 \times 1)$ and $c(4 \times 2)$ structures by using the relation with the corresponding work function change ΔW[30]: i.e. $\Delta p_z = \frac{\Delta W(\varepsilon_0 A)}{e}$, where A is the surface area of $p(2 \times 1)$ unit cell and ΔW between the $p(2 \times 1)$ and $c(4 \times 2)$ structures is 0.456 eV. We find that the variation of E_b with respect to the external electric field of $0 \leq |\mathbf{E}| \leq 0.5$ V/Å is less than ~20 meV, much smaller than that (~160 meV) obtained from hole doping (see Fig. 3). Thus, we can say that the influence of hole doping on E_b is much more pronounced than that arising from external electric field.

It should be noted that, in order to explain their observed symmetric-dimer STM images, Yokoyama and Takayanagi[15] suggested that anharmonic potential effects would reduce the barrier height to induce the dynamical dimer flipping. However, this mechanism cannot explain the STM observations of buckled and symmetric dimer images depending on the polarity of the bias voltage[17,21–24]. Moreover, according to the DFT calculation of Bokes *et al.*[31], the energy difference ΔE between the symmetric and buckled dimer structures varies by only ~0.01 eV/dimer with changing the lattice parameter of ±1%. Since this value of ΔE is much smaller than those obtained in the present case of charge doping, the energy change associated with the negative thermal expansion is unlikely to explain the observed symmetric-dimer STM images.

To account for the symmetric dimer images observed from low-temperature STM experiments[15–17,21], we investigate the flip-flop motion of buckled dimers driven by either thermal activation[32] or quantum tunneling. For this, we employ a symmetric double-well potential [see Fig. 1(b)] that describes the potential energy surface of flipping dimers as a function of θ. This potential surface is confirmed by the nudged elastic band calculations[33,34] for $n_e = 0$, $0.3e$, and $-0.3e$, where the $p(2 \times 1)$ structure is in unstable equilibrium, showing that there is no energy barrier between the $p(2 \times 1)$ and $c(4 \times 2)$ structures. Using a harmonic approximation, we obtain a vibration frequency for this potential well as $f_0 = \frac{\omega}{2\pi} = \frac{1}{2\pi}\sqrt{\frac{k}{I}} \approx 0.3 \times 10^{13}\ \mathrm{sec}^{-1}$ in the absence of electron or hole doping, where the torsion constant k and the inertia moment I of flipping dimer can be estimated from $E_b = k\theta_0^2$ (θ_0: dimer buckling angle at the lowest-energy configuration) and $I = \frac{1}{2} m_{\mathrm{si}} d_D^2$ (m_{si}: mass of Si atom). Based on an Arrhenius-type activation process, a thermally excited flipping rate can be expressed as $f_T = f_0 \exp\left(\frac{-E_b}{kT}\right)$. With the calculated values of E_b and f_0 as a function of $|n_e| \leq 0.6e$, we obtain f_T smaller than $0.8 \times 10^{-36}\ \mathrm{sec}^{-1}$ at 10 K. This thermal flipping rate is too small to explain the observed symmetric-dimer STM images with flicker noise[15,16]. As an alternative explanation for the flip-flop motion of buckled dimers, we consider quantum tunneling (QT) within the double-well potential, whose flipping rate can be approximated[35,36] as

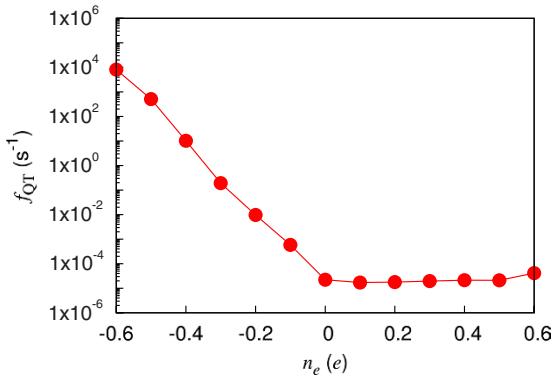

Figure 4. Calculated QT-driven flipping rate of buckled dimers as a function of electron and hole dopings.

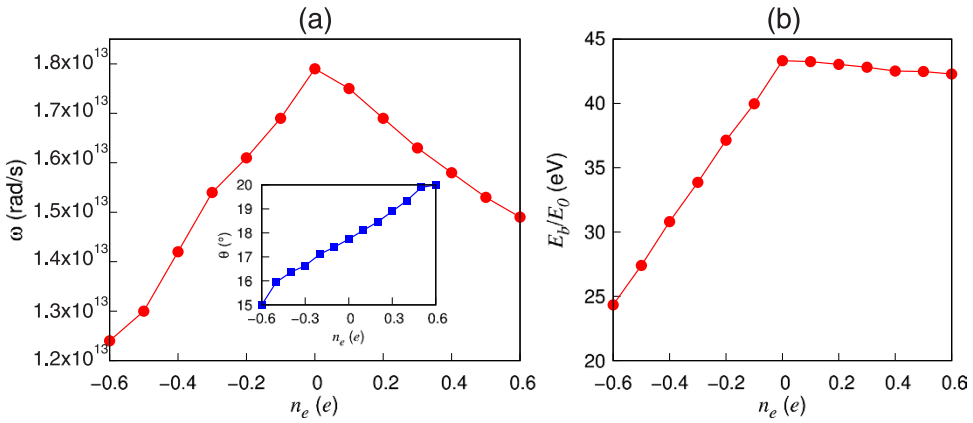

Figure 5. (**a**) Zero-point frequency ω and (**b**) the ratio of the energy barrier E_b and the zero-point energy $E_0\left(=\frac{1}{2}\hbar\omega\right)$. The inset in (**a**) shows the dimer buckling angle as a function of electron and hole dopings.

$$f_{QT} = \sqrt{\frac{8E_b\omega}{\hbar\pi}}\exp\left(\frac{-2E_b}{\hbar\omega}\right). \quad (1)$$

Contrasting with f_T, f_{QT} is independent of temperature, while it is determined by the ratio of E_b and the zero-point energy $E_0\left(=\frac{1}{2}\hbar\omega\right)$. In Fig. 4, the estimated values of f_{QT} are plotted as a function of n_e. We find that f_{QT} sharply increases with increasing hole doping, while it is nearly flat with respect to electron doping. Here, we note that ω obtained from the calculated values of E_b and θ_0 [see Fig. 5(a)] gives rise to a large decrease in the ratio of E_b and E_0 under hole doping, but hardly changes E_b/E_0 under electron doping [see Fig. 5(b)]. Since hole doping with $n_e = -0.6e$ gives a relatively smaller ratio of $E_b/E_0 \sim 23$ compared to that (~42) over the entire range of electron doping, f_{QT} significantly increases by eight orders of magnitude upon hole doping (see Fig. 4). For hole doping with $|n_e| > 0.5e$, f_{QT} becomes greater than $\sim 5.1 \times 10^2\,\mathrm{sec}^{-1}$. Considering that it takes $\tau_{\mathrm{dimer}} \approx 10^{-2}$ sec to obtain an STM image of a dimer[37,38], such a hole-doping induced flip-flop motion can produce the observed symmetric dimer images in low-temperature STM experiments[15–17,21]. It is noted that, as temperature increases above ~40 K, surface charging effects begin to disappear, therefore giving rise to $f_{QT} \sim 2.2 \times 10^{-5}\,\mathrm{sec}^{-1}$ computed at $n_e = 0$ (see Fig. 4). This indicates that the QT-driven flipping motion becomes weakened above ~40 K, leading to the appearance of buckled-dimer STM images. In particular, Manzano *et al.*'s observation[21] of buckled dimer images at voltages lower than −1.5 V can be explained by the fact that the hole doping induced by small negative bias voltages can reduce the energy barrier E_b, but not so much so that the flip-flop motion is enabled to produce symmetric dimer images. Meanwhile, according to the low-temperature STM experiment of Yoshida *et al.*[39], the flip-flop frequency depends both on gap voltage and tunneling current. Here, we note that at positive bias voltages the dynamic behavior of the dimers was observable. Interestingly, such effects of gap voltage and tunneling current in STM measurement was observed in a different surface system Sn/Ge(111)[40]. It is noticeable that, according to Yoshida *et al.*'s STM experiment[39], the flip-flop frequency as a function of the positive-bias voltage and tunneling current (between 0.2 nA and 1 nA) is relatively much smaller than that as a function of the negative-bias voltage. This difference of the flip-flop frequency with respect to the bias-polarity is not only qualitatively consistent with the present simulation results, but it may also explain why some STM experiments[17,21,22] easily observed the symmetric dimer images with negative-bias voltages. Also, the relatively smaller flip-flop frequency as a

function of tunneling current may provide an explanation for why Ono *et al.*'s STM experiment[17] observed no change of images with respect to tunneling current below 0.3 nA.

We note that the application of **E** along the $-z$ ($+z$) direction decreases (increases) E_b. Consequently, one expects that negative sample bias (equivalently, negative electric field) inducing hole doping at low temperature enhances the magnitude of f_{QT}. On the other hand, positive sample bias (positive electric field) inducing electron doping suppresses f_{QT}. These drastically different aspects of negative and positive bias voltages in low-temperature STM experiments account for the observations of symmetric and buckled dimer images in filled-state and empty-state images, respectively[17,21].

Although we present a simple picture of the QT-driven flip-flop motion of buckled dimers with a double-well potential, we believe that it captures the microscopic mechanism underlying low-temperature symmetric-dimer STM images, as explained above. It is noted that the present DFT-GGA calculation may tend to somewhat overestimate the energy gain due to buckling. Indeed, the quantum Monte Carlo calculation[41] which accurately describes electronic correlations extrapolates the value of E_b up to ~150 meV per dimer, in good agreement with the experimental estimates[32]. This reduction of E_b can enhance the QT-driven flip-flop motion of buckled dimers.

Conclusions

In conclusion, we have performed a DFT-GGA calculation for the Si(001) surface to investigate the energy difference between the symmetric-dimer structure and the $c(4 \times 2)$ structure under electron or hole doping as well as applied external electric field along the [001] direction. This energy difference corresponding to the energy barrier for the flipping of buckled dimers was found to decrease more significantly with respect to hole doping compared to electron doping. Consequently, we found that hole doping gives rise to a sizable QT-driven frequency of the flip-flop motion of buckled dimers while electron doping shows the marginal QT effects. These different QT aspects of hole and electron dopings are most likely to yield the imaging difference between the filled- and empty-state STM images at low temperature. Thus, we concluded that quantum tunneling enhanced by the tunneling-induced hole doping causes the observation of symmetric dimer images in low-temperature STM experiments, but, as temperature increases, such a surface charging effect becomes weakened, thereby leading to an appearance of asymmetric dimer images.

Methods

The present DFT calculations were performed using the FHI-aims code[42] for an accurate, all-electron description based on numeric atom-centered orbitals, with "tight" computational settings. For the exchange-correlation energy, we employed the generalized gradient approximation of Perdew-Burke-Ernzerhof (PBE)[43]. The Si(001) surafce (with the Si lattice constant $a_0 = 5.418$ Å) was modeled by a twelve-layer slab with ~30 Å of vacuum in between the slabs, where each Si atom in the bottom layer was passivated by two H atoms. The k-space integrations for the $p(2 \times 1)$ and $c(4 \times 2)$ structures were done equivalently with 32 k points in the surface Brillouin zone of the $p(2 \times 1)$ unit cell. Here, for the total-energy calculation of the $c(4 \times 2)$ structure, we employed the equivalent $p(4 \times 2)$ unit cell whose surface area is twice as large as that of the $c(4 \times 2)$ structure. We used a dipole correction that cancels the artificial electric field across the slab. All atoms except the bottom two layers were allowed to relax along the calculated forces until all the residual force components were less than 0.02 eV/Å. For the simulation of surface charging, we used the virtual crystal approximation[44] to compensate excess electrons n_e or holes, where the nuclear charge of Si atoms is modified by a small amount $\Delta Z = n_e/N$ (N: number of Si atoms within four deeper atomic layers). We note that all the simulations with hole or electron doping have been performed without spin-polarization. In order to check the possibility of spin-polarization, we performed the spin-polarized simulations for the doping concentrations of $|n_e| \leq 0.6e$. We found that the ground structure is nonmagnetic in the range of $|n_e| \leq 0.5e$, but it becomes spin-polarized at $|n_e| = 0.6e$ with a small magnetic moment of ~0.1 μB. However, in the latter spin-polarized cases, the energy barrier between the $p(2 \times 1)$ and $c(4 \times 2)$ structures changes little by less than ~1 meV compared to the corresponding nonmagnetic cases.

References

1. Dabrowski, J. & Müssig, H.-J. *Silicon Surfaces and Formation of Interfaces* (World Scientific, Singapore, 2000).
2. Chadi, D. J. Atomic and Electronic Structures of Reconstructed Si(100) Surfaces. *Phys. Rev. Lett.* **43,** 43 (1979).
3. Krüger, P. & Pollmann, J. Dimer Reconstruction of Diamond, Si, and Ge(001) Surfaces. *Phys. Rev. Lett.* **74,** 1155 (1995).
4. Yates, J. T., Jr. A new opportunity in silicon-based microelectronics. *Science* **279,** 335–336 (1998).
5. Medeiros-Ribeiro, G., Bratkovski, A. M., Kamins, T. I., Ohlberg, D. A. A. & Williams, R. S. Shape Transition of Germanium Nanocrystals on a Silicon (001) Surface from Pyramids to Domes. *Science* **279,** 353–355 (1998).
6. Wolkow, R. A. Controlled molecular adsorption on silicon: laying a foundation for molecular devices. *Annu. Rev. Phys. Chem.* **50,** 413–441 (1999).
7. Engelund, M. *et al.* Tunneling spectroscopy of close-spaced dangling-bond pairs in Si(001):H. *Sci. Rep.* **5,** 14496 (2015).
8. Qiu, Y. *et al.* Epitaxial diamond-hexagonal silicon nano-ribbon growth on (001) silicon. *Sci. Rep.* **5,** 12692 (2015).
9. Tromp, R. M., Hamers, R. J. & Demuth, J. E. Si(001) Dimer Structure Observed with Scanning Tunneling Microscopy. *Phys. Rev. Lett.* **55,** 1303 (1985).
10. Ramstad, A., Brocks, G. & Kelly, P. J. Theoretical study of the Si(100) surface reconstruction. *Phys. Rev. B* **51,** 14504 (1995).
11. Kipp, L., Biegelsen, D. K., Northrup, J. E., Swartz, L.-E. & Bringans, R. D. Reflectance Difference Spectroscopy: Experiment and Theory for the Model System Si(001): As and Application to Si(001). *Phys. Rev. Lett.* **76,** 2810 (1996).
12. Shirasawa, T., Mizuno, S. & Tochihara, H. Electron-Beam-Induced Disordering of the Si(001)-$c(4 \times 2)$ Surface Structure. *Phys. Rev. Lett.* **94,** 195502 (2005).
13. Wolkow, R. A. Direct Observation of an Increase in Buckled Dimers on Si(001) at Low Temperature. *Phys. Rev. Lett.* **68,** 2636 (1992).
14. Kondo, Y., Amakusa, T., Iwatsuki, M. & Tokumoto, H. Phase transition of the Si(001) surface below 100 K. *Surf. Sci.* **453,** L318–L322 (2000).
15. Yokoyama, T. & Takayanagi, K. Anomalous flipping motions of buckled dimers on the Si(001)surface at 5 K. *Phys. Rev. B* **61,** R5078 (2000).
16. Mitsui, T. & Takayanagi, K. Extrinsic structure changes by STM at 65 K on Si(001). *Phys. Rev. B* **62,** R16251 (2000).

17. Ono, M. *et al.* Dimer buckling of the Si(001)2 × 1 surface below 10 K observed by low-temperature scanning tunneling microscopy. *Phys. Rev. B* **67,** 201306 (2003).
18. Perdigão, L. *et al.* Semiconducting Surface Reconstructions of p-Type Si(100) Substrates at 5 K. *Phys. Rev. Lett.* **92,** 216101 (2004).
19. Kawai, H. & Narikiyo, O. Vibration of the Dimer on Si(001) Surface Excited by STM Current. *J. Phys. Soc. Jpn.* **73,** 417–422 (2004).
20. Hata, K., Yoshida, S. & Shigekawa, H. $p(2 \times 2)$ Phase of Buckled Dimers of Si(100) Observed on n-Type Substrates below 40 K by Scanning Tunneling Microscopy. *Phys. Rev. Lett.* **89,** 286104 (2002).
21. Manzano, C., Soe, W. H., Kawai, H., Saeys, M. & Joachim, C. Origin of the apparent 2 × 1 topography of the Si(100)-$c(4 \times 2)$ surface observed in low-temperature STM images. *Phys. Rev. B* **83,** 201302(R) (2011).
22. Riedel, D., Lastapis, M., Martin, M. G. & Dujardin, G. Influence of tip-surface interactions and surface defects on Si(100) surface structures by low-temperature (5 K) scanning tunneling microscopy. *Phys. Rev. B* **69,** 121301(R) (2004).
23. Sagisaka, K., Kitahara, M., Fujita, D., Kido, G. & Koguchi, N. Scanning tunnelling microscopy in extreme fields: very low temperature, high magnetic field, and extreme high vacuum. *Nanotechnology* **15,** S371–S375 (2004).
24. Sagisaka, K., Fujita, D. & Kido, G. Phase Manipulation between $c(4 \times 2)$ and $p(2 \times 2)$ on the Si(100) Surface at 4.2 K. *Phys. Rev. Lett.* **91,** 146103 (2003).
25. Brihuega, I. *et al.* Direct Observation of a 3 × 3 Phase in α-Pb/Ge(111)at 10 K. *Phys. Rev. Lett.* **95,** 206102 (2005).
26. Polei, S. *et al.* Structural Transition in Atomic Chains Driven by Transient Doping. *Phys. Rev. Lett.* **111,** 156801 (2013).
27. Seino, K., Schmidt, W. G. & Bechstedt, F. Energetics of Si(001) Surfaces Exposed to Electric Fields and Charge Injection. *Phys. Rev. Lett.* **93,** 036101 (2004).
28. Zhang, H. *et al.* Stabilization and Manipulation of Electronically Phase-Separated Ground States in Defective Indium Atom Wires on Silicon. *Phys. Rev. Lett.* **113,** 196802 (2014).
29. Haiss, W. Surface stress of clean and adsorbate-covered solids. *Rep. Prog. Phys.* **64,** 591 (2001).
30. Leung, T. C., Kao, C. L., Su, W. S., Feng, Y. J. & Chan, C. T. Relationship between surface dipole, work function and charge transfer: Some exceptions to an established rule. *Phys. Rev. B* **68,** 195408 (2003).
31. Bokes, P., Štich, I. & Mitas, L. Ground-state reconstruction of the Si(001) surface:symmetric versus buckled dimers. *Chem. Phys. Lett.* **362,** 559–566 (2002).
32. Hata, K., Sainoo, Y. & Shigekawa, H. Atomically Resolved Local Variation of the Barrier Height of the Flip-Flop Motion of Single Buckled Dimers of Si(100). *Phys. Rev. Lett.* **86,** 3084 (2001).
33. Henkelman, G., Uberuaga, B. P. & Jónsson, H. A climbing image nudged elastic band method for finding saddle points and minimum energy paths. *J. Chem. Phys.* **113,** 9901–9904 (2000).
34. Henkelman, G. & Jónsson, H. Improved tangent estimate in the nudged elastic band method for finding minimum energy paths and saddle points. *J. Chem. Phys.* **113,** 9978–9985 (2000).
35. Ronci, F., Colonna, S. & Cricenti, A. Evidence of Sn Adatoms Quantum Tunneling at the α-Sn/Si(111)Surface. *Phys. Rev. Lett.* **99,** 166103 (2007).
36. Merzbacher, E. *Quantum Mechanics* (J. Wiley, New York, 1970).
37. Cho, J.-H. & Kim, K. S. Metastable phase of symmetric dimers on Si(001). *Phys. Rev. B* **69,** 125312 (2004).
38. Fukaya, Y. & Shigeta, Y. Phase Transition from Asymmetric to Symmetric Dimer Structure on the Si(001) Surface at High Temperature. *Phys. Rev. Lett.* **91,** 126103 (2003).
39. Yoshida, S. *et al.* Probe effect in scanning tunneling microscopy on Si(100) low-temperature phases. *Phys. Rev. B* **70,** 235411 (2004).
40. Colonna, S., Ronci, F., Cricenti, A. & Le Lay, G. Metallic Nature of the α-Sn/Ge(111) Surface down to 2.5 K. *Phys. Rev. Lett.* **101,** 186102 (2008).
41. Healy, S. B., Filippi, C., Kratzer, P., Penev, E. & Scheffler, M. Role of Electronic Correlation in the Si(100) Reconstruction: A Quantum Monte Carlo Study. *Phys. Rev. Lett.* **87,** 016105 (2001).
42. Blum, V. *et al. Ab initio* molecular simulations with numeric atom-centered orbitals. *Comput. Phys. Commun.* **180,** 2175–2196 (2009).
43. Perdew, J. P., Burke, K. & Ernzerhof, M. Generalized Gradient Approximation Made Simple. *Phys. Rev. Lett.* **77,** 3865 (1996).
44. Richter, N. A. *et al.* Concentration of Vacancies at Metal-Oxide Surfaces: Case Study of MgO(100). *Phys. Rev. Lett.* **111,** 045502 (2013).

Acknowledgements

We thank Prof. Changgan Zeng, Prof. Shun-Fang Li, and Prof. Zhenyu Zhang for helpful discussions. This work was supported by the National Basic Research Program of China (Grant No. 2012CB921300), National Natural Science Foundation of China (Grants No. 11274280, No.11504332 and No. 61434002), and National Research Foundation of Korea (Grant No. 2015R1A2A2A01003248). The calculations were performed by KISTI supercomputing center through the strategic support program (KSC-2015-C3-017) for the supercomputing application research.

Author Contributions

X.-Y.R., Y.J. and J.-H.C. designed the study and wrote the paper; X.-Y.R. and H.-J.K. carried out first-principles simulations; C.-Y.N. participated in analyzing of the data; all authors discussed the results and contributed to the manuscript.

Additional Information

Supplementary information accompanies this paper at http://www.nature.com/srep

Competing financial interests: The authors declare no competing financial interests.

How to cite this article: Ren, X.-Y. *et al.* Origin of Symmetric Dimer Images of Si(001) Observed by Low-Temperature Scanning Tunneling Microscopy. *Sci. Rep.* **6**, 27868; doi: 10.1038/srep27868 (2016).